HHS Public Access

Author manuscript

Nat Neurosci. Author manuscript; available in PMC 2010 January 01.

Published in final edited form as:

Nat Neurosci. 2009 July ; 12(7): 848–856. doi:10.1038/nn.2322.

Regulation of Acetylcholine Receptor Clustering by ADF/Cofilin-Directed Vesicular Trafficking

Chi Wai Lee[1,2], **Jianzhong Han**[2], **James R. Bamburg**[3], **Liang Han**[1,2], **Rachel Lynn**[1], and **James Q. Zheng**[1,2]

[1]Department of Cell Biology, Emory University School of Medicine, Atlanta, Georgia 30322

[2]Department of Neuroscience and Cell Biology, University of Medicine and Dentistry of New Jersey, Robert Wood Johnson Medical School, Piscataway, New Jersey 08854

[3]Department of Biochemistry and Molecular Biology, and Molecular, Cellular and Integrative Neuroscience Program, Colorado State University, Fort Collins, Colorado 80523

Summary

Postsynaptic receptor localization is crucial for synapse development and function, but the underlying cytoskeletal mechanisms remain elusive. Using *Xenopus* neuromuscular junctions as a model, we here report that actin depolymerizing factor (ADF)/cofilin regulates actin-dependent vesicular trafficking of acetylcholine receptors (AChRs) to the postsynaptic membrane. We found that active ADF/cofilin was concentrated in small puncta adjacent to AChR clusters and spatiotemporally correlated with the formation and maintenance of surface AChR clusters. Importantly, increased actin dynamics, vesicular markers, and intracellular AChRs were all enriched at the sites of ADF/cofilin localization. Furthermore, a substantial amount of new AChRs was detected at these ADF/cofilin-enriched sites. Manipulation of either ADF/cofilin activity through its serine-3 phosphorylation or ADF/cofilin localization via 14-3-3 proteins markedly attenuated AChR insertion and clustering. These results suggest that spatiotemporally restricted ADF/cofilin-mediated actin dynamics regulate AChR trafficking during the development of neuromuscular synapses.

Keywords

ADF/cofilin; receptor trafficking; actin dynamics; neuromuscular junction; synapse

Correspondence: James Zheng, Ph.D., Department of Cell Biology, Emory University School of Medicine, 615 Michael Street, Atlanta, GA 30322. Tel: (404) 727-9133. Fax: (404) 727-6256. Email: james.zheng@emory.edu.

Author contributions: CWL designed and performed most of the experiments, data analyses, and manuscript writing. JH did the electrophysiological recording. JRB provided insightful advice to the experiments and critical input to the manuscript, as well as contributed the reagents for ADF/cofilin and 14-3-3ζ. LH and RL performed the molecular subcloning of some of the DNA constructs used. JQZ formulated and oversaw the research project, and directed the experiments, analyses, and writing.

Introduction

Chemical synapses represent a major form of neuronal connections in the vertebrate nervous system that underlie a wide spectrum of neural functions. A prominent feature of chemical synapses is the presence of a postsynaptic apparatus containing highly concentrated receptors for effective reception of neurotransmitters released from the presynaptic nerve terminal. Regulation of postsynaptic receptor localization is therefore crucial for synapse formation, function, and modulation 1–3. At present, the cellular mechanisms underlying the spatiotemporal control of receptor trafficking and clustering at the postsynaptic site remain poorly understood. The neuromuscular junction (NMJ), because of its size, accessibility and simplicity 4, offers a good model to study the spatial distribution and trafficking of postsynaptic acetylcholine receptors (AChRs). Previous studies have shown that aneural AChR clusters can spontaneously form in the absence of innervation and nerve-secreted factors *in vivo* 5. Nerve innervation, however, induces site-directed clustering of AChRs through the re-distribution from aneural clusters, recruitment of diffuse receptors, and new synthesis from the sub-synaptic nuclei 4, 6. Two counteracting nerve-derived factors, agrin and acetylcholine, regulate the redistribution of AChRs on the muscle membrane 7. Agrin activates muscle-specific tyrosine kinase (MuSK) for inducing AChR clustering on the postsynaptic membrane 8, whereas acetylcholine disperses extra-synaptic AChR clusters 9, 10.

It remains unclear how AChRs are spatiotemporally delivered to the synaptic site during synapse formation. Passive diffusion-trap and/or active trafficking mechanisms may be involved in AChR re-distribution 11, 12. Clustered AChRs are believed to be immobilized via scaffolding connections to the actin cytoskeleton 13, 14, thus their re-distribution likely requires dynamic changes in the cortical actin network. In this study, we used a combination of live cell imaging, molecular and pharmacological manipulations to investigate the cytoskeletal control of AChR trafficking during synapse formation. We find that actin depolymerizing factor (ADF)/cofilin plays an important role in synaptic targeting of AChRs. Our data show that ADF/cofilin accumulates at the nascent synaptic site prior to the clustering of surface AChRs. Furthermore, the disassembly of the spontaneous AChR clusters is preceded by the disappearance of active ADF/cofilin aggregates. Localized ADF/cofilin is associated with increased dynamic actin turnover and spatially correlates with the surface delivery of intracellular AChRs through vesicular trafficking. We further identify that 14-3-3 molecules are essential for the spatial localization of ADF/cofilin to regulate AChR trafficking. Finally, alteration of ADF/cofilin activity or disruption of its localization prevents the formation of new AChR clusters induced by synaptogenic stimuli. These findings indicate that spatiotemporally restricted ADF/cofilin-regulated actin dynamics regulate the surface targeting of postsynaptic receptors at synaptic sites.

Results

Active ADF/cofilin localizes at AChR clusters

Nerve-independent AChR clusters can spontaneously develop on muscle surface in culture on matrix-coated substrate and display an elaborately perforated pattern with a striking similarity to synaptic AChR clusters at the NMJs *in vivo* 4, 15. Similarly, spontaneous

AChR clusters were observed in embryonic *Xenopus* muscle cells cultured on laminin-containing attachment matrix 16, as visualized by live labeling with rhodamine-conjugated α-bungarotoxin (Rh-BTX) (Fig. 1a). To examine a role for ADF/cofilin in AChR clustering, we labeled AChRs in live cells with Rh-BTX, followed by fixation and immunostaining of either the total *Xenopus* ADF/cofilin (XAC) or the inactive phosphoserine-3 XAC (pXAC) 17. The specificity of these antibodies was verified by our previous studies 18, 19 and XAC expression in *Xenopus* muscle tissues was confirmed by RT-PCR and western blotting (Supplementary Fig. 1). We found that XAC was preferentially concentrated as small puncta at the AChR-poor perforations within the spontaneous AChR clusters, whereas pXAC exhibited a uniform distribution (Fig. 1b). This striking complementary pattern of XAC and AChR distributions was also observed by live imaging of muscle cells expressing GFP-XAC in conjunction with AChR labeling (Fig. 1b). Moreover, the localization of GFP-XAC to the AChR-poor perforations was further enhanced by the constitutively active mutation (3A; serine-3 replaced by alanine), but markedly reduced by the inactive mutation (3E; serine-3 replaced by glutamate) (Supplementary Fig. 2). It should be noted that the observed XAC puncta are unlikely a result of membrane infoldings as seen in mature NMJs, since staining with a volume dye DTAF 20 showed no apparent spatial patterns associated with the spontaneous AChR clusters (Fig. 1b). The DTAF fluorescence intensity, however, reduced at the location of a yolk granule inside the cell indicating its effectiveness in highlighting the cell volume. Furthermore, confocal imaging revealed that GFP-XAC was localized as puncta underneath the plasma membrane without obvious membrane infoldings (Supplementary Fig. 3a). Together, these results indicate that putatively active, nonphosphorylated XAC is preferentially enriched in AChR-poor perforations within these complex structures of spontaneous AChR clusters.

We next tested if XAC accumulates at the site of AChR clustering during synapse formation. We found that beads coated with an active recombinant agrin C-terminal fragment 21 potently induced AChR clustering (Fig. 1c), whereas control BSA-coated or full-length agrin-coated beads were ineffective 22 (Supplementary Fig. 4). Immunostaining showed that XAC accumulated at the agrin bead-muscle contact in a “ring” pattern surrounding the AChR clusters, whereas pXAC distributed uniformly (Fig. 1c). A similar pattern of XAC and AChR localization was also observed by live imaging of GFP-XAC and AChR (Fig. 1c and Supplementary Fig. 3b). Occasionally, GFP-XAC puncta could be detected at the bead-muscle contact where no AChR clusters had yet been formed (Fig. 1c), suggesting a potential temporal difference in the localization of XAC and AChRs induced by agrin beads. We also examined the localization of XAC at neuromuscular synapses in *Xenopus* nerve-muscle co-cultures. Live imaging showed that GFP-XAC puncta were distributed closely with AChR clusters along the nerve-contacted trail on the muscle cell (Fig. 1d). At higher magnifications, XAC puncta and AChR clusters were localized in a juxtaposing, non-overlapping pattern. In some cases, XAC was also enriched at the AChR-poor perforations in the nerve-induced AChR clusters, showing a similar complementary topography to that of spontaneous AChR clusters. Together, these results show that active, non-phosphorylated XAC localizes to AChR clusters in the spontaneous or synaptic specializations.

Spontaneous AChR clusters undergo slow re-distribution in culture (Supplementary Fig. 5), allowing the examination of a spatiotemporal correlation between ADF/cofilin localization and AChR re-distribution. In a time-lapse recording, GFP-XAC was first found to concentrate in the perforations of a spontaneous AChR cluster (Fig. 2a). Over the course of 40 h recording, this AChR cluster re-distributed to a new location. Apparently, GFP-XAC puncta were detected at the new location at 10 h, whereas detectable AChR clusters were not observed until 20 h. Intriguingly, the disappearance of localized GFP-XAC at the original AChR cluster was found to precede the gradual disassembly of the AChR clusters. This spatiotemporal relationship was better demonstrated after AChR clusters and GFP-XAC puncta were highlighted with red and green pseudo-colors, respectively.

At developing NMJs, nerve-induced AChR clustering on the postsynaptic membrane is accompanied by the dispersal of the spontaneous AChR clusters 23. We therefore performed the similar time-lapse recordings in muscle cells under agrin bead stimulation. In this case, GFP-XAC became localized at the bead contact site as early as 2 h after stimulation, whereas no AChR clusters were detected at the same site until 4 h (Fig. 2b). Concurrently, we observed a significant loss of GFP-XAC signals in the spontaneous AChR clusters at 8 h, which later dispersed gradually. The pseudocolor highlighted AChR and XAC signals clearly show that the re-distribution of AChRs was preceded by that of XAC from the spontaneous clusters to the bead-induced site. By monitoring 6 individual agrin bead-induced clusters at a higher temporal resolution (one frame every 15 min for 4 h after bead stimulation), we detected the formation of GFP-XAC puncta prior to that of AChR clusters at 5 out of 6 bead-induced sites, whereas in only one case both GFP-XAC and AChR clusters were detected at the same time. The times taken after bead stimulation for the detection of GFP-XAC and AChR clusters were 77.5 ± 16.2 (s.e.m.) min and 110.0 ± 18.0 (s.e.m.) min respectively (Supplementary Fig. 6a). The appearance of XAC at agrin bead contacts and its disappearance at the spontaneous AChR clusters exhibit a reciprocal temporal correlation that coincide with the formation of new AChR clusters and dispersal of old ones (Supplementary Fig. 6b). Therefore, XAC localization in the nascent postsynaptic sites induced by agrin might direct the formation of AChR clusters, and the maintenance of spontaneous AChR clusters may also require localized XAC.

Localized ADF/cofilin increases actin dynamic turnover

One potential function for locally concentrated XAC is to regulate the actin dynamics. When labeled with fluorescent phalloidin, filamentous (F-) actin (*Total*) was found at the perforations in the spontaneous AChR clusters (Fig. 3a), but actin-enriched myofibrils obscured the details concerning its association with AChR clusters. To selectively label newly formed F-actin, we masked existing F-actin with a membrane-permeable actin-binding drug, jasplakinolide 13, as it competes with phalloidin for F-actin binding 24. When jasplakinolide-treated muscle cells were recovered in drug-free medium for 4 h, fluorescent phalloidin signals were largely diminished in myofibrils, but enriched at the cell peripheral and the AChR-poor perforations in the spontaneous clusters, suggesting that new F-actin was preferentially generated at these locations over the 4 h period.

We next labeled F-actin barbed ends by exposing the cells to rhodamine-actin in a mild detergent saponin 25. We consistently found actin barbed ends concentrated at AChR-poor perforations in the spontaneous AChR clusters (Fig. 3a). The close relationship between XAC and actin barbed ends was reflected by its high co-localization coefficient in the triple staining of AChR, XAC and actin barbed ends (Supplementary Fig. 7). We also labeled the monomeric globular (G-) actin with Vitamin D-binding proteins 26 and found local enrichment of endogenous G-actin at those perforations in AChR clusters (Fig. 3a). These results suggest that the actin cytoskeleton in the perforated regions of spontaneous AChR clusters undergoes dynamic turnover. This hypothesis was tested by photo-activation and live imaging of muscle cells expressing photo-activatable GFP-actin (paGFP-actin) 27. When the muscle cell was globally exposed to an UV light, paGFP-actin fluorescence illuminated myofibrils of the entire cells (Fig. 3b), demonstrating the effective photo-activation. Upon local activation around spontaneous AChR clusters, paGFP-actin fluorescence declined much faster in the perforated region than that in the AChR area (Fig. 3c), suggesting a faster turnover rate for F-actin at these sites (Fig. 3d and Supplementary Video 1). Similarly, we found that actin barbed ends and G-actin were distributed in a “ring” pattern surrounding the bead-induced AChR clusters (Fig. 3e). Photo-activation/imaging of paGFP-actin also showed a higher turnover rate for the actin cytoskeleton adjacent to the AChR clusters (Fig. 3f,g and Supplementary Video 2). These observations indicate that XAC-associated dynamic actin remodeling likely plays a role in spatial targeting of AChRs, rather than in anchoring and stabilization of surface receptors.

Vesicular AChRs accumulate at ADF/cofilin localization

To test a possible involvement of XAC-mediated actin dynamics in vesicular trafficking of AChRs, we first used FM4-64 staining to probe membrane recycling 28. We found that FM4-64 signals appeared as puncta in the AChR-poor perforations of the spontaneous clusters (Fig. 4a). Immunostaining of EEA1, an early endosomal marker 29, also showed local enrichment of endosomal vesicles in those perforations. We also found that, similar to XAC, FM4-64-labeled puncta and EEA1 signals accumulated around the agrin bead-induced AChR clusters (Fig. 4b). To test if membrane recycling is involved in AChR clustering, we applied phenylarsine oxide (PAO), a general inhibitor of receptor-mediated endocytosis 30, and found that it abolished both the formation of agrin-induced AChR clusters and the dispersal of spontaneous AChR clusters (Supplementary Fig. 8a). Since PAO also inhibits tyrosine phosphatases 31, we employed low temperature (4 °C) treatment to inhibit membrane fusion and vesicular trafficking 32. Interestingly, the low temperature inhibited the re-distribution of AChR, not XAC, induced by the agrin bead. Finally, monodansylcadaverine (MDC), a clathrin-dependent endocytosis inhibitor 33, had no effect on agrin-induced localization of XAC and AChR (Supplementary Fig. 8b). These findings suggest that spatially localized XAC may regulate the actin dynamics to control the vesicular trafficking of AChRs in clathrin-independent mechanisms.

We next examined the presence of an internal pool of AChRs and its contribution to the surface AChRs using a double labeling approach (see Methods and Supplementary Fig. 9a). We detected a substantial pool of internal AChRs associated with the spontaneous AChR clusters. Importantly, these intracellular AChRs appeared as discrete puncta at centers of

those AChR-poor perforations of the spontaneous clusters (Fig. 4c). The spatial segregation of surface and internal pools of AChRs was clearly depicted in a 3D intensity profile. We also applied the same approach to examine agrin-induced AChR clusters and detected internal AChRs accumulated at the periphery surrounding the surface AChR clusters (Fig. 4d).

Since XAC, dynamic actin, vesicular compartments, and intracellular AChRs are colocalized, we suspected that new AChRs are inserted to the surface at these locations. To test this, we sequentially labeled the existing surface AChRs (old) with Rh-BTX and newly inserted AChRs (new) with Alexa 488-BTX (see Methods and Supplementary Fig. 9b). If the second labeling was immediately after the first one, no signal of new AChRs was detected (Fig. 5a). If we performed the second labeling at 4 h afterward, new AChRs were detected both at AChR-poor perforations and in the AChR-rich regions (Fig. 5a). The new AChRs in mix with the old ones might result from their initial insertion into the AChR-poor perforations, followed by rapid re-distribution and incorporation into the existing pools. To test this, we performed the same procedure, but imaged both old and new AChRs at additional time points. The initial pair of images at 4 h showed a substantial portion of new AChRs that did not overlap with the old ones, but became intermingled over time (Fig. 5b). We quantified the size of new AChRs in the perforations and normalized it against the total perforation area (green dots in area B) (Fig. 5c). The incorporation and/or insertion of new AChRs into old AChR clusters was similarly quantified and normalized against the total old AChR clusters (yellow dots in area A). We found that the amount of new AChRs in the perforations of the clusters decreased from 4 h to 20 h, which was accompanied by a gradual increase in the incorporation and/or insertion of new AChRs into the old AChR clusters. Additionally, the Pearson's co-localization coefficient between these two pools of surface AChRs had significantly increased over time. We further tested if old and new AChRs induced by agrin beads are spatially segregated using the same approach. We found that newly inserted AChRs over the first 4 h agrin-bead stimulation were mainly localized at the periphery of the old AChR clusters; however, these two pools of AChRs became mixed by 20 h (Fig. 5d). The time-dependent co-localization of old and new AChRs induced by agrin beads is supported by an increase in the Pearson's co-localization coefficient (Fig. 5e). These data suggest that a substantial amount of new AChRs is inserted at the XAC-enriched AChR-poor regions in the spontaneous and agrin-induced clusters, which becomes gradually incorporated into the existing pool of AChRs.

ADF/cofilin regulates synaptic development

The depolymerizing/severing activity of ADF/cofilin is regulated by the phosphorylation state of its serine-3 residue 17, which can be mutated for over-expression to interfere with the endogenous ADF/cofilin activity. The effects of these XAC mutants on actin polymerization during neurite outgrowth have been previously characterized in cultured cortical neurons 34. We found that over-expression of 3A (constitutively active) or 3E (inactive), but not wild-type (WT), form of GFP-XAC reduced AChR clusters at the agrin bead contacts (Fig. 6a,b). Similarly, we found that muscle cells expressing GFP-XAC showed extensive AChR clusters along the nerve-contacted trails, which was markedly reduced by over-expression of XAC-3A or -3E (Fig. 6c). The area of AChR clusters per unit

length of nerve-muscle contact was significantly reduced in muscle cells over-expressing GFP-XAC in 3A or 3E form, when compared to cells over-expressing WT form or control muscle cells (Fig. 6d).

We next performed whole-cell patch-clamp recordings of spontaneous synaptic currents (SSCs) in neuron-muscle co-culture 35. In co-cultures of muscle cells expressing different forms of GFP-XAC (M^+) and wild-type spinal neurons (N^-), we found that expression of XAC-3A and XAC-3E in muscle cells reduced SSCs (Supplementary Fig. 10). The decrease in the SSC amplitude is consistent with the reduced AChRs found along the nerve-muscle contacts after the expression of XAC-3A or 3E. The reduction in the frequency of SSCs by XAC-3E expression might result from XAC-3E inhibition of retrograde signaling that affects presynaptic transmitter release. Nonetheless, these data provide evidence that ADF/cofilin phosphocycling on the serine-3 residue regulates AChR clustering and synaptic function.

14-3-3 mediates XAC localization and AChR clustering

The 14-3-3 family of phosphoproteins is known for its scaffolding role in subcellular targeting of intracellular signals 36. Among at least seven mammalian isoforms, ADF/cofilin interacts with 14-3-3ζ and 14-3-3ε *in vitro* 37. We expressed GFP-14-3-3ζ in muscle cells and examined its distribution and effects on AChR clustering. Interestingly, when GFP-14-3-3ζ was expressed at a low level, it was enriched at the perforated regions in the spontaneous AChR clusters (Fig. 7a). In some cases, we observed largely scattered AChR clusters but with a small region of concentrated AChRs, at where GFP-14-3-3ζ was only found to localize to the small concentrated AChR area. At high GFP-14-3-3ζ expression level, however, most of the spontaneous AChR clusters exhibited a scattered pattern without preferential localization of GFP-14-3-3ζ. Similar effects of GFP-14-3-3ζ over-expression on agrin bead-induced AChR clustering were also observed (Fig. 7b). Intriguingly, GFP-14-3-3ζ over-expression also diminished the XAC localization in agrin bead-muscle contacts.

To further investigate the role of 14-3-3ζ in ADF/cofilin localization and AChR clustering, we knocked down *Xenopus* 14-3-3ζ expression by morpholino antisense oligonucleotides. The effectiveness of 14-3-3ζ morpholino knockdown was confirmed by western blotting using an antibody recognizing *Xenopus* 14-3-3ζ/β (Fig. 7c). In muscle cells with 14-3-3ζ morpholino (as evidenced by fluorescent dextran signals), we found that the spontaneous AChR clusters were also scattered as small aggregates (Fig. 7d). Consistently, morpholino knockdown of 14-3-3ζ also blocked AChR clustering and XAC localization induced by agrin beads (Fig. 7e). Quantitative analysis showed that either over-expression of GFP-14-3-3ζ at high level or knockdown of endogenous 14-3-3ζ expression in muscle cells disrupted the compact pattern of the spontaneous AChR clusters and reduced the percentage of AChR occupied area (Fig. 7f). Similarly, AChR clustering induced by agrin beads was also significantly attenuated (Fig. 7g). These results thus suggest that 14-3-3ζ is involved in the spatial localization of ADF/cofilin for AChR clustering.

To better understand the relationship between ADF/cofilin localization and surface targeting of AChRs, we tested if manipulation of either ADF/cofilin activity (by over-expression of

XAC mutants) or its localization (by 14-3-3ζ morpholino knockdown) affects the surface insertion of new AChRs. Due to the technical limit for triple staining, we masked all surface AChRs on the muscle cells with a saturating dose of unlabeled BTX (see Fig. 5a for the masking effectiveness). After 4 h agrin bead stimulation, the muscle cells were labeled with Rh-BTX and subsequently fixed for visualization and quantification of newly inserted AChRs. We found that over-expression of GFP-XAC had no influence on surface insertion of new AChRs induced by agrin beads. But in muscle cells expressing XAC mutants or 14-3-3ζ morpholino, the amount of new AChR clusters was significantly reduced at the bead-induced sites (Fig. 8a,b). Similarly, AChR insertion to the membrane surface at the spontaneous clusters was also attenuated by the over-expression of XAC mutants or 14-3-3ζ morpholino knockdown (Fig. 8c,d). Therefore, disruption of ADF/cofilin localization or activity impairs AChR surface insertion.

Discussion

Regulated trafficking of postsynaptic receptors represents a major mechanism underlying synaptic plasticity 1, 3, but the cytoskeletal involvement is not well understood. In this study, we show that spatiotemporally restricted ADF/cofilin-mediated actin dynamics regulate the trafficking and surface targeting of AChRs to the nascent postsynaptic sites at developing NMJs. Our findings indicate that, on top of the passive diffusion-trap mechanism, an active receptor trafficking mechanism may underlie the re-distribution of AChRs from the spontaneous clusters to the nascent postsynaptic sites during synaptogenic stimulation. We hypothesize that, upon synaptogenic induction, AChRs are endocytosed from the spontaneous AChR clusters, which, together with the new synthesized AChRs, may be transported and delivered to the nascent postsynaptic sites for insertion. During this process, ADF/cofilin may lead the way to localize to the nascent sites (through 14-3-3 scaffolding activated by synaptogenic signals) to modulate local dynamic actin cytoskeleton that defines, assists, and/or maintains vesicular fusion and recycling of AChRs (see Supplementary Fig. 11).

F-actin is considered as a cytoskeletal scaffold for the docking and anchorage of structural and signaling molecules to the postsynaptic sites at NMJs 14, 38. Our data here have elucidated a novel function for ADF/cofilin-mediated actin dynamics in spatiotemporal regulation of AChR trafficking and clustering. The enrichment of new F-actin, actin barbed ends, and G-actin in locations adjacent to, but not overlapped with, surface AChR clusters in the spontaneous and synaptic specializations argue against that ADF/cofilin-mediated actin dynamics function as a stable scaffold for receptor anchorage and immobilization. The co-localization of these dynamic actin regions with the vesicular pool of internal AChRs, together with the presence of newly inserted surface AChRs in these regions, indicates that the spatially restricted dynamic actin may actively regulate the vesicular trafficking of AChRs to and from the membrane. Dynamic actin turnover has been known to regulate vesicular membrane trafficking 39, 40. Local increased dynamic actin turnover by ADF/cofilin may break the cortical actin barrier and/or actively facilitate the vesicle fusion to the plasma membrane. The permissive and active roles for dynamic actin in vesicular trafficking of AChRs are not exclusive and may cooperate for spatial control of AChR delivery to the postsynaptic site. Interestingly, we observed a compact cluster of ADF/cofilin at early time

points after agrin bead stimulation when AChR clusters had yet been formed, which subsequently was transformed into a ring structure surrounding AChR clusters. Similar to the central synapses 2, it is conceivable that ADF/cofilin-mediated vesicular trafficking (especially the exocytosis) of postsynaptic receptors is restricted at the receptor-poor peri-synaptic sites for effective modulation of postsynaptic receptor density.

Recent studies suggest that a high concentration of active cofilin favors F-actin nucleation 41, 42. The localization of active, non-phosphorylated ADF/cofilin at sites of newly polymerized F-actin with elevated levels of barbed ends and endogenous G-actin suggests that ADF/cofilin may sever the existing F-actin and contribute to the abundant supply of actin monomers and barbed ends for rapid actin assembly in the spontaneous and synaptic AChR clusters. The suppression of AChR clustering by over-expression of either constitutively active or inactive ADF/cofilin indicates that phosphocycling-dependent regulation of localized ADF/cofilin is required for its function in dynamzing the actin cytoskeleton for AChR trafficking. This can also be explained by a “set-point” hypothesis whereby hyper- or hypo-activity of ADF/cofilin may imbalance the actin dynamics and the proper trafficking of AChRs to the postsynaptic membrane. Moreover, the finding that constitutively active GFP-XAC-3A accumulates in the perforations of spontaneous AChR clusters (Supplementary Fig. 2), but not to the agrin-induced AChR clusters (Fig. 6a) indicates that disruption of ADF/cofilin phosphocycling may also impair its translocation in response to agrin signaling. Previous studies have shown that agrin-MuSK signaling involves p21-activated kinase (PAK1) 43, an activator of LIM kinases 44. LIM kinases are the major kinases that phosphorylate and inactivate ADF/cofilin 45. It is thus reasonable to speculate that both ADF/cofilin activity and translocation may be regulated by phosphocycling, which may be targeted by agrin-MuSK signaling.

We also presented evidence that the 14-3-3 family of scaffolding proteins is involved in ADF/cofilin localization. Both serine-3 phosphorylated and non-phosphorylated ADF/cofilin binds to 14-3-3, although the former has a higher affinity. Moreover, phosphorylation on the serine-23 or -24 residue of ADF/cofilin appears to be sufficient for its 14-3-3 binding 37. Therefore, ADF/cofilin localization via 14-3-3 molecules does not necessarily depend on its activity. At present, only 14-3-3ζ and 14-3-3ε have been reported to interact with ADF/cofilin *in vitro* 37, 46, but other isoforms may interact with ADF/cofilin because of the high homology of 14-3-3 family members 47. Intriguingly, 14-3-3γ co-localizes and potentially interacts with MuSK at adult NMJs 48. Whether 14-3-3γ regulates ADF/cofilin localization for actin-dependent AChR trafficking remains to be investigated. Besides interacting directly with ADF/cofilin, 14-3-3 also interacts with the upstream regulators of ADF/cofilin, LIM kinase 46 and Slingshot phosphatase 45. Collectively, 14-3-3 may spatially localize both ADF/cofilin and its regulators to the synaptic sites to coordinately control the dynamic actin turnover for AChR trafficking. Finally, additional synapse-specific scaffolding proteins may also participate in ADF/cofilin localization.

In conclusion, our work has identified a novel role for ADF/cofilin in postsynaptic receptor trafficking and clustering. Our findings indicate that ADF/cofilin may spatiotemporally regulate the trafficking and surface delivery of AChRs during neuromuscular synaptogenesis. Intriguingly, ADF/cofilin is also concentrated at the periphery of the

postsynaptic density at the central synapses 49 and is involved in the trafficking of growth factor receptors in invasive tumor cells 50. Therefore, it is exciting to speculate that ADF/cofilin-mediated actin dynamics may play an important role in receptor trafficking underlying a broad range of cell functions.

Methods

Microinjection and primary culture preparation from *Xenopus* embryos

DNA constructs encoding GFP-XAC WT/3A/3E 34, and GFP-14-3-3ζ, or paGFP-actin were microinjected into one blastomere of 2-cell stage *Xenopus* embryos. Typically, each embryo was injected with 20-100 pg of DNA. To knock down the expression of 14-3-3ζ, custom-designed morpholino antisense oligonucleotides (5'-CTGGACCAGTTCATTTTTATCCATG-3'; Gene Tools) were co-injected with a cell linage tracer Oregon Green 488-dextran (Invitrogen) into the 1- or 2-cell stage embryos. GFP- or dextran-expressing embryos were screened for primary culture preparation. Myotomal muscle tissues and neural tubes were dissected from stage 19-22 *Xenopus* embryos after collagenase treatment as previously described 16. Dissociated muscle cells were plated on glass coverslips coated with laminin-containing matrix, ECL (Millipore) and grown in culture medium containing 10% (vol/vol) Leibovitz's L-15 medium (Invitrogen), 87% (vol/vol) Steinberg's solution (60 mM NaCl, 0.67 mM KCl, 0.35 mM, Ca(NO3)2, 0.83 mM $MgSO_4$, 10 mM HEPES, pH 7.4), 1% (vol/vol) fetal bovine serum, 1% (vol/vol) Penicillin/Streptomycin and 1% (vol/vol) Gentamicin sulfate. Unless specified, the muscle cultures were kept at ~18 °C for at least 5 d before experiments to minimize the presence of yolk granules. To make nerve-muscle co-cultures, dissociated spinal neurons were plated on 5 d-old muscle cultures for the induction of synaptogenesis.

All the experiments involving *Xenopus* frogs and embryos were carried out in accordance to the NIH guideline for animal use and have been approved by the INSTITUTIONAL ANIMAL CARE AND USE COMMITTEE (IACUC) of UMDNJ-RWJMS and Emory University.

RT-PCR analysis of XAC expression in *Xenopus* myotomal muscle tissues

Dissociated muscle tissues from two *Xenopus* embryo at stage 19-22 were dissected and lysed for the synthesis of the first stand cDNA by the SuperScript III Cells Direct cDNA Synthesis kit (Invitrogen). A pair of specific primers for the XAC sequence was designed as follows: 5'-TCTCTCAAAACCATAGGCACT-3' (forward) and 5'-ACAGGAATTTCGACACCCTC-3' (reverse). PCR products were resolved in ethidium bromide-stained agarose gels. We expected a band of PCR products at a molecular weight of 236 base pairs if XAC mRNA is presence in the muscle tissues.

Visualization of newly polymerized F-actin, free actin barbed ends and G-actin

To visualize the newly polymerized F-actin, the less dynamic form of F-actin (enriched mainly in myofibrils) was masked with a cell-permeable actin-binding drug jasplakinolide (Invitrogen) at 10 μM for 3 h in live muscle cells 13. After recovery in drug-free medium, the treated cells were fixed, permeabilized, and then newly polymerized actin filaments were

probed by fluorescein phalloidin (Invitrogen). Free F-actin barbed ends were labeled by 0.45 μM rhodamine-conjugated G-actin (Cytoskeleton) for 3 min in the saponin permeabilization solution (20 Mm HEPES, 138 mM KCl, 4 mM $MgCl_2$, 3 mM EGTA, 0.2 mg/ml saponin, 1 mM ATP, and 1% BSA, pH 7.5) 25. The labeled cells were fixed with 2% paraformaldehyde (PFA) immediately after labeling procedures for imaging. Endogenous G-actin labeling was performed as previously described 26. In short, muscle cells were fixed with 4% PFA for 10 min, and then extracted in cold acetone for 5 min. The cells were incubated with 10 μg/ml Vitamin-binding protein DBP (Calbiochem) for 1 h, followed by the standard immunofluorescence protocol with an anti-DBP polyclonal antibody (Dako).

FM dye staining

To visualize constitutive vesicular recycling in muscle cells, we exposed the cells to 5 μg/ml FM4-64 (Invitrogen) in culture medium for 30 min. Labeled cells were washed twice with ice-cold calcium- and magnesium-free Hank's Balanced Salt Solution (HBSS; Invitrogen), and then examined live by fluorescence microscopy.

Identification of different pools of AChRs

To differentiate surface and internal AChRs, surface AChRs were labeled with 0.1 μM rhodamine-conjugated BTX (Invitrogen) for 45 min and followed by a saturating dose (6 μM) of unlabeled BTX (Invitrogen) for 15 min. The cells were fixed with 4% PFA and permeabilized with 0.5% Triton X-100. After blocking with 5% BSA for 1 h, the internal pool of AChRs was labeled with 1 μM Alexa 488-conjuated BTX (Invitrogen) for 1 h. To differentiate existing (old) and newly inserted (new) AChR clusters in live cultured muscle cells, old AChRs were labeled with 0.1 μM rhodamine-conjugated BTX and saturated with 6 μM unlabeled BTX. After bead stimulation or recovery in culture medium, new AChRs were labeled with 1 μM Alexa 488-conjugated BTX for 45 min. A schematic illustration of these two labeling methods is provided in Supplementary Fig. 9.

Immunocytochemistry and immunoblotting

For immunofluorescent experiments, *Xenopus* muscle or nerve-muscle cultures were fixed with 4% PFA and 0.25% glutaraldehyde for 15 min and followed by permeabilization with 0.5% Triton X-100 for 10 min. For immunostaining of pXAC, we increased the fixation time to 45 min to maximally preserve pXAC signals. The fixed cultures were blocked with 5% BSA for at least 1 h. They were then stained with the primary antibodies for 2 h and followed by the fluorescent secondary antibodies for 45 min. The coverslips were mounted on slides with an anti-fade agent Fluoromount-G (SouthernBiotech). For immunoblotting experiments, stage 19-22 *Xenopus* embryos were homogenized in the lysis buffer (50 mM Tris-HCl, pH 7.4, 150 mM NaCl, 1 mM EDTA, 1% Triton X-100, 1 mM PMSF, 1 mg/ml aprotinin, 1 mg/ml leupeptin, and 1 mg/ml pepstatin). The protein lysates were resolved by 12% Tris-Glycine pre-cast gels (Invitrogen) and transferred to nitrocellulose membranes, which were blocked in PBST with 10% milk for 1 h and then immunoblotted with primary rabbit anti-14-3-3ζ/β antibodies (Millipore) for 1 h. The primary antibodies were detected by HRP-conjugated secondary antibodies and enhanced chemiluminescence substrate. The

membranes were stripped for 15 min with the Restore Plus Western Blot stripping buffer (Thermo) and reprobed with GADPH antibodies (Santa Cruz).

Fluorescence microscopy and time-lapse imaging

Fluorescent imaging was performed on an inverted microscope (TE2000; Nikon) using a 60× N.A. 1.4 Plan Apo or a 100× N.A. 1.3 Super Fluor (in photoactivation experiments) objective with identical settings between the control and experimental groups. Digital still or time-lapse images were captured with a CCD camera (SensiCam QE; Cooke Scientific) using the IPLab imaging software (BD Biosciences). Confocal imaging was done on a Nikon inverted microscope (TE300) equipped with a Nikon C1 confocal unit using a 60× N.A.1.4 Plan Apo objective.

Electrophysiology

Dissociated muscle cells and spinal neurons were plated on plain glass coverslips. Spontaneous synaptic currents (SSCs) were recorded from innervated muscle cells in 1 d-old nerve-muscle co-cultures by the whole-cell recording methods at room temperature. The recording solution contained 140 mM NaCl, 5 mM KCl, 1 mM, $CaCl_2$, 1 mM $MgCl_2$, 10 mM HEPES, pH 7.4. The intra-pipette solution contained 145 mM KCl, 1 mM NaCl, 1 mM $MgCl_2$, 1 mM Mg-ATP, 10 mM HEPES, pH 7.2. The membrane potentials of the muscle cells recorded were voltage clamped at –70 mV. All data were collected by an Axopatch 200B patch clamp amplifier (Molecular Devices). The frequency of SSCs was defined as the number of SSC events per minute. The amplitudes of SSCs were analyzed using the Strathclyde electrophysiology software (University of Strathclyde).

Data and statistical analyses

Data are reported as means ± s.e.m. unless otherwise indicated. Quantitative measurement, 3D intensity profiles, and pseudocolored threshold images were performed using the ImageJ software (National Institute of Health). Statistical comparison of data sets was performed by two-tailed Student's *t* test.

Supplementary Material

Refer to Web version on PubMed Central for supplementary material.

Acknowledgments

We would like to thank Dr. Bai Lu (National Institute of Child Health and Human Development) for his help in our electrophysiological experiments. This work is supported by grants from National Institutes of Health to JQZ (GM083889 and AG029596) and JRB (NS40371). CWL was supported by a postdoctoral fellowship from The Croucher Foundation (Hong Kong, China).

References

1. Bredt DS, Nicoll RA. AMPA receptor trafficking at excitatory synapses. Neuron. 2003; 40:361–379. [PubMed: 14556714]
2. Kennedy MJ, Ehlers MD. Organelles and trafficking machinery for postsynaptic plasticity. Annu Rev Neurosci. 2006; 29:325–362. [PubMed: 16776589]

3. Song I, Huganir RL. Regulation of AMPA receptors during synaptic plasticity. Trends Neurosci. 2002; 25:578–588. [PubMed: 12392933]
4. Sanes JR, Lichtman JW. Development of the vertebrate neuromuscular junction. Annu Rev Neurosci. 1999; 22:389–442. [PubMed: 10202544]
5. Lin W, et al. Distinct roles of nerve and muscle in postsynaptic differentiation of the neuromuscular synapse. Nature. 2001; 410:1057–1064. [PubMed: 11323662]
6. Sanes JR, Lichtman JW. Induction, assembly, maturation and maintenance of a postsynaptic apparatus. Nat Rev Neurosci. 2001; 2:791–805. [PubMed: 11715056]
7. Misgeld T, Kummer TT, Lichtman JW, Sanes JR. Agrin promotes synaptic differentiation by counteracting an inhibitory effect of neurotransmitter. Proc Natl Acad Sci U S A. 2005; 102:11088–11093. [PubMed: 16043708]
8. DeChiara TM, et al. The receptor tyrosine kinase MuSK is required for neuromuscular junction formation in vivo. Cell. 1996; 85:501–512. [PubMed: 8653786]
9. Lin W, et al. Neurotransmitter acetylcholine negatively regulates neuromuscular synapse formation by a Cdk5-dependent mechanism. Neuron. 2005; 46:569–579. [PubMed: 15944126]
10. Chen F, et al. Rapsyn interaction with calpain stabilizes AChR clusters at the neuromuscular junction. Neuron. 2007; 55:247–260. [PubMed: 17640526]
11. Peng HB, Zhao DY, Xie MZ, Shen ZW, Jacobson K. The role of lateral migration in the formation of acetylcholine receptor clusters induced by basic polypeptide-coated latex beads. Dev Biol. 1989; 131:197–206. [PubMed: 2909404]
12. Camus G, Jasmin BJ, Cartaud J. Polarized sorting of nicotinic acetylcholine receptors to the postsynaptic membrane in Torpedo electrocyte. Eur J Neurosci. 1998; 10:839–852. [PubMed: 9753152]
13. Dai Z, Luo X, Xie H, Peng HB. The actin-driven movement and formation of acetylcholine receptor clusters. J Cell Biol. 2000; 150:1321–1334. [PubMed: 10995438]
14. Hall ZW, Lubit BW, Schwartz JH. Cytoplasmic actin in postsynaptic structures at the neuromuscular junction. J Cell Biol. 1981; 90:789–792. [PubMed: 7026578]
15. Kummer TT, Misgeld T, Lichtman JW, Sanes JR. Nerve-independent formation of a topologically complex postsynaptic apparatus. J Cell Biol. 2004; 164:1077–1087. [PubMed: 15037598]
16. Peng HB, Baker LP, Chen Q. Tissue culture of Xenopus neurons and muscle cells as a model for studying synaptic induction. Methods Cell Biol. 1991; 36:511–526. [PubMed: 1811149]
17. Bamburg JR. Proteins of the ADF/cofilin family: essential regulators of actin dynamics. Annu Rev Cell Dev Biol. 1999; 15:185–230. [PubMed: 10611961]
18. Shaw AE, et al. Cross-reactivity of antibodies to actin- depolymerizing factor/cofilin family proteins and identification of the major epitope recognized by a mammalian actin-depolymerizing factor/cofilin antibody. Electrophoresis. 2004; 25:2611–2620. [PubMed: 15300782]
19. Wen Z, et al. BMP gradients steer nerve growth cones by a balancing act of LIM kinase and Slingshot phosphatase on ADF/cofilin. J Cell Biol. 2007; 178:107–119. [PubMed: 17606869]
20. Schindelholz B, Reber BF. Quantitative estimation of F-actin in single growth cones. Methods. 1999; 18:487–492. [PubMed: 10491279]
21. Bowe MA, Fallon JR. The role of agrin in synapse formation. Annu Rev Neurosci. 1995; 18:443–462. [PubMed: 7605069]
22. Daggett DF, Stone D, Peng HB, Nikolics K. Full-length agrin isoform activities and binding site distributions on cultured Xenopus muscle cells. Mol Cell Neurosci. 1996; 7:75–88. [PubMed: 8812060]
23. Kuromi H, Kidokoro Y. Nerve disperses preexisting acetylcholine receptor clusters prior to induction of receptor accumulation in Xenopus muscle cultures. Dev Biol. 1984; 103:53–61. [PubMed: 6714520]
24. Bubb MR, Senderowicz AM, Sausville EA, Duncan KL, Korn ED. Jasplakinolide, a cytotoxic natural product, induces actin polymerization and competitively inhibits the binding of phalloidin to F-actin. J Biol Chem. 1994; 269:14869–14871. [PubMed: 8195116]
25. Schafer DA, et al. Visualization and molecular analysis of actin assembly in living cells. J Cell Biol. 1998; 143:1919–1930. [PubMed: 9864364]

26. Cao LG, Fishkind DJ, Wang YL. Localization and dynamics of nonfilamentous actin in cultured cells. J Cell Biol. 1993; 123:173–181. [PubMed: 8408196]
27. Patterson GH, Lippincott-Schwartz J. A photoactivatable GFP for selective photolabeling of proteins and cells. Science. 2002; 297:1873–1877. [PubMed: 12228718]
28. Cochilla AJ, Angleson JK, Betz WJ. Monitoring secretory membrane with FM1-43 fluorescence. Annu Rev Neurosci. 1999; 22:1–10. [PubMed: 10202529]
29. Mu FT, et al. EEA1, an early endosome-associated protein. EEA1 is a conserved alpha-helical peripheral membrane protein flanked by cysteine "fingers" and contains a calmodulinbinding IQ motif. J Biol Chem. 1995; 270:13503–13511. [PubMed: 7768953]
30. Hertel C, Coulter SJ, Perkins JP. A comparison of catecholamine-induced internalization of beta-adrenergic receptors and receptor-mediated endocytosis of epidermal growth factor in human astrocytoma cells. Inhibition by phenylarsine oxide. J Biol Chem. 1985; 260:12547–12553. [PubMed: 2995380]
31. Dai Z, Peng HB. A role of tyrosine phosphatase in acetylcholine receptor cluster dispersal and formation. J Cell Biol. 1998; 141:1613–1624. [PubMed: 9647653]
32. Tsuji S. Electron-microscope cytochemistry of acetylcholine-like cation by means of low-temperature "ionic fixation". Histochemistry. 1984; 81:453–455. [PubMed: 6520022]
33. Schutze S, et al. Inhibition of receptor internalization by monodansylcadaverine selectively blocks p55 tumor necrosis factor receptor death domain signaling. J Biol Chem. 1999; 274:10203–10212. [PubMed: 10187805]
34. Meberg PJ, Bamburg JR. Increase in neurite outgrowth mediated by overexpression of actin depolymerizing factor. J Neurosci. 2000; 20:2459–2469. [PubMed: 10729326]
35. Evers J, Laser M, Sun YA, Xie ZP, Poo MM. Studies of nerve-muscle interactions in Xenopus cell culture: analysis of early synaptic currents. J Neurosci. 1989; 9:1523–1539. [PubMed: 2723739]
36. Fu H, Subramanian RR, Masters SC. 14-3-3 proteins: structure, function, and regulation. Annu Rev Pharmacol Toxicol. 2000; 40:617–647. [PubMed: 10836149]
37. Gohla A, Bokoch GM. 14-3-3 regulates actin dynamics by stabilizing phosphorylated cofilin. Curr Biol. 2002; 12:1704–1710. [PubMed: 12361576]
38. Luther PW, Samuelsson SJ, Bloch RJ, Pumplin DW. Cytoskeleton-membrane interactions at the postsynaptic density of Xenopus neuromuscular junctions. J Neurocytol. 1996; 25:417–427. [PubMed: 8866242]
39. Sokac AM, Bement WM. Kiss-and-coat and compartment mixing: coupling exocytosis to signal generation and local actin assembly. Mol Biol Cell. 1495; 17:1495–1502. [PubMed: 16436510]
40. Eitzen G. Actin remodeling to facilitate membrane fusion. Biochim Biophys Acta. 2003; 1641:175–181. [PubMed: 12914958]
41. Andrianantoandro E, Pollard TD. Mechanism of actin filament turnover by severing and nucleation at different concentrations of ADF/cofilin. Mol Cell. 2006; 24:13–23. [PubMed: 17018289]
42. Chen H, et al. In vitro activity differences between proteins of the ADF/cofilin family define two distinct subgroups. Biochemistry. 2004; 43:7127–7142. [PubMed: 15170350]
43. Luo ZG, et al. Regulation of AChR clustering by Dishevelled interacting with MuSK and PAK1. Neuron. 2002; 35:489–505. [PubMed: 12165471]
44. Edwards DC, Sanders LC, Bokoch GM, Gill GN. Activation of LIM-kinase by Pak1 couples Rac/Cdc42 GTPase signalling to actin cytoskeletal dynamics. Nat Cell Biol. 1999; 1:253–259. [PubMed: 10559936]
45. Soosairajah J, et al. Interplay between components of a novel LIM kinase-slingshot phosphatase complex regulates cofilin. Embo J. 2005; 24:473–486. [PubMed: 15660133]
46. Birkenfeld J, Betz H, Roth D. Identification of cofilin and LIM-domain-containing protein kinase 1 as novel interaction partners of 14-3-3 zeta. Biochem J. 2003; 369:45–54. [PubMed: 12323073]
47. Lau JM, Wu C, Muslin AJ. Differential role of 14-3-3 family members in Xenopus development. Dev Dyn. 2006; 235:1761–1776. [PubMed: 16607644]
48. Strochlic L, et al. 14-3-3 gamma associates with muscle specific kinase and regulates synaptic gene transcription at vertebrate neuromuscular synapse. Proc Natl Acad Sci U S A. 2004; 101:18189–18194. [PubMed: 15604144]

49. Racz B, Weinberg RJ. Spatial organization of cofilin in dendritic spines. Neuroscience. 2006; 138:447–456. [PubMed: 16388910]

50. Nishimura Y, Yoshioka K, Bernard O, Bereczky B, Itoh K. A role of LIM kinase 1/cofilin pathway in regulating endocytic trafficking of EGF receptor in human breast cancer cells. Histochem Cell Biol. 2006; 126:627–638. [PubMed: 16763828]

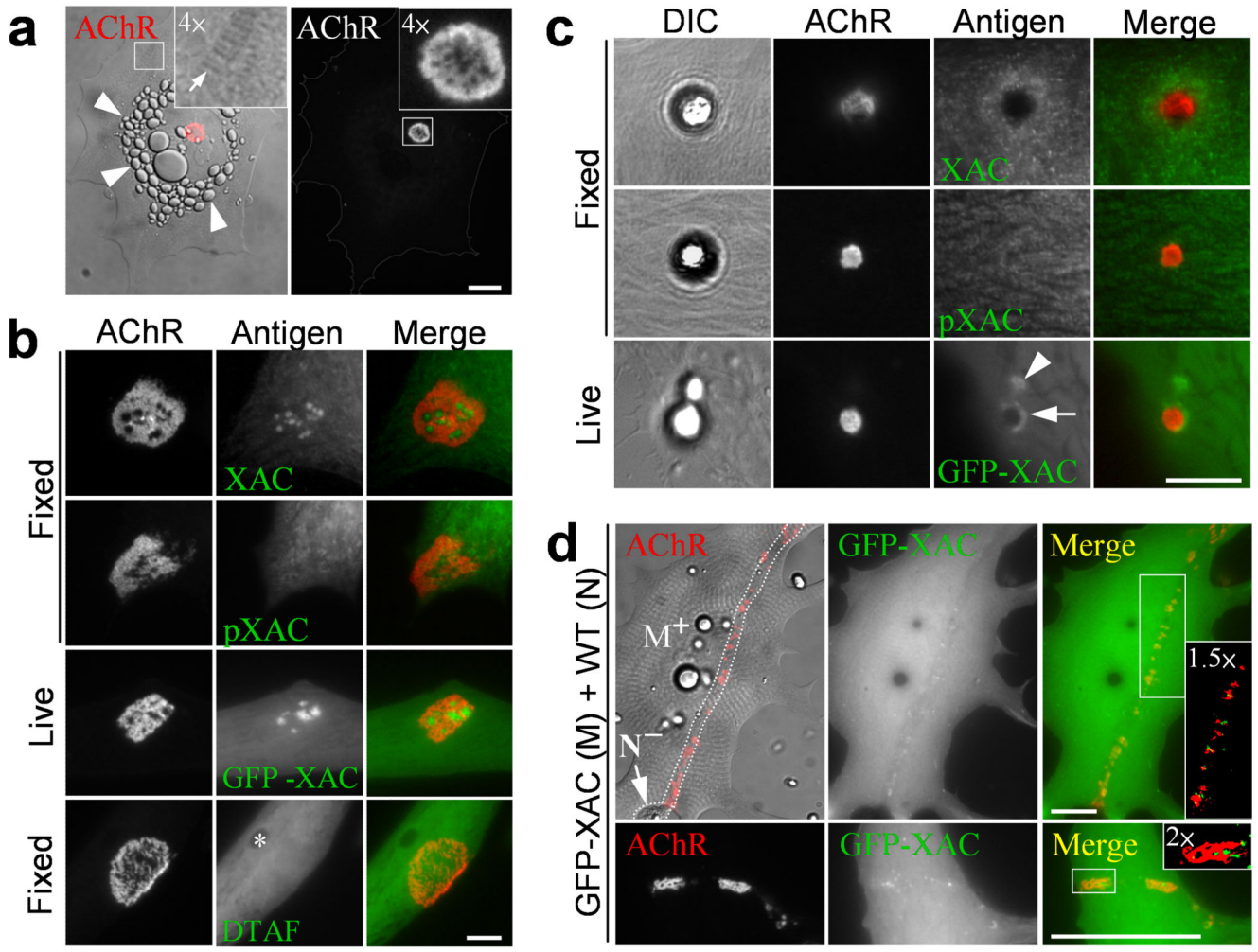

Figure 1. Localization of ADF/cofilin in spontaneous and synaptic AChR clusters

(**a**) Representative DIC and fluorescent images of a 1-d old cultured *Xenopus* muscle cell showing spontaneous AChR clusters after Rh-BTX labeling. Insets: magnified regions. Arrow: striation; arrowheads: yolk granules. (**b**) The spatial pattern of spontaneous AChR clusters and XAC in *Xenopus* muscle cells after 5 d in culture. First and second rows: the distribution of AChRs (Rh-BTX labeling) and endogenous XAC and pXAC (immunostaining). Third row: the distribution of AChRs and GFP-XAC in a live muscle cell. Last row: AChR distribution and the cell volume labeled by DTAF. Asterisk: a site of volume reduction caused by a yolk granule. (**c**) Agrin bead-induced AChR clustering and XAC localization as revealed by immunostaining in fixed cells or live imaging. Arrow: GFP-XAC accumulation around the AChR clusters induced by an agrin bead. Arrowhead: GFP-XAC accumulation at an agrin bead contact even without AChRs. (**d**) The spatial distributions of AChR clusters and GFP-XAC at developing neuromuscular junctions in culture. GFP-XAC-expressing muscle cells (M^+) were co-cultured with wild-type spinal neurons (N^-) for 3 d. The nerve-muscle contacts were outlined by the dotted lines in the DIC image, which was overlaid with Rh-BTX-labeled AChR signals (red). Another example of AChR clusters and GFP-XAC signals from a different cell was shown in the bottom row.

Insets: the boxed region was magnified and pseudo-colored after an intensity threshold. Scale bars: 40 μm (a, d); 10 μm (b, c).

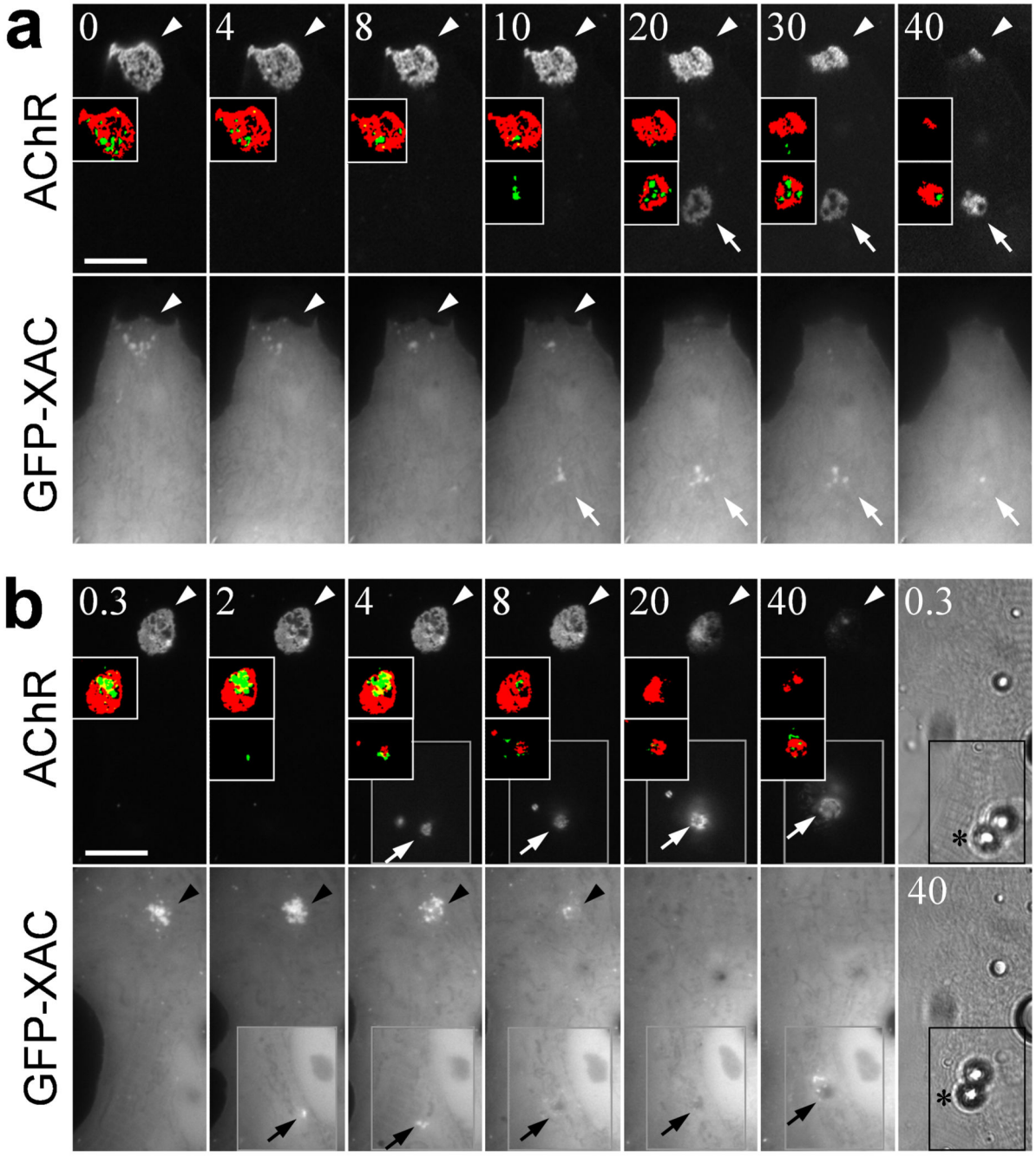

Figure 2. Dynamics of ADF/cofilin in spontaneous and agrin-induced re-distribution of AChRs

(**a**) A time-lapse series showing the dynamic re-distribution of GFP-XAC and AChRs in two spontaneous clusters. AChRs were labeled with Rh-BTX before the start of recordings. For a better clarity, pseudo-colored images after an intensity threshold were shown in the insets. Arrowheads: the position of the original spontaneous cluster; arrows: the position of a newly formed spontaneous cluster. Numbers indicate elapsed time (in hour) in the recordings. (**b**) A time-lapse series showing the dynamics of GFP-XAC in the formation and dispersal of agrin-induced and spontaneous AChR clusters, respectively. Muscle cells were labeled with

Rh-BTX and then stimulated by agrin beads at 0 h. Pairs of pseudo-colored images after intensity threshold were shown in the insets. Gray boxed regions were focused on the top of muscle cells where agrin beads made contacts with the muscle membrane. DIC images from the start and end of the recordings were included in the last column to show a slight lateral movement of beads (asterisks) on the muscle surface during the 40 h time-lapse recordings. Arrowheads: the position of the spontaneous cluster; arrows: the position of the bead-induced specialization. Numbers indicate time (in hour) after bead stimulation. Scale bars: 20 μm.

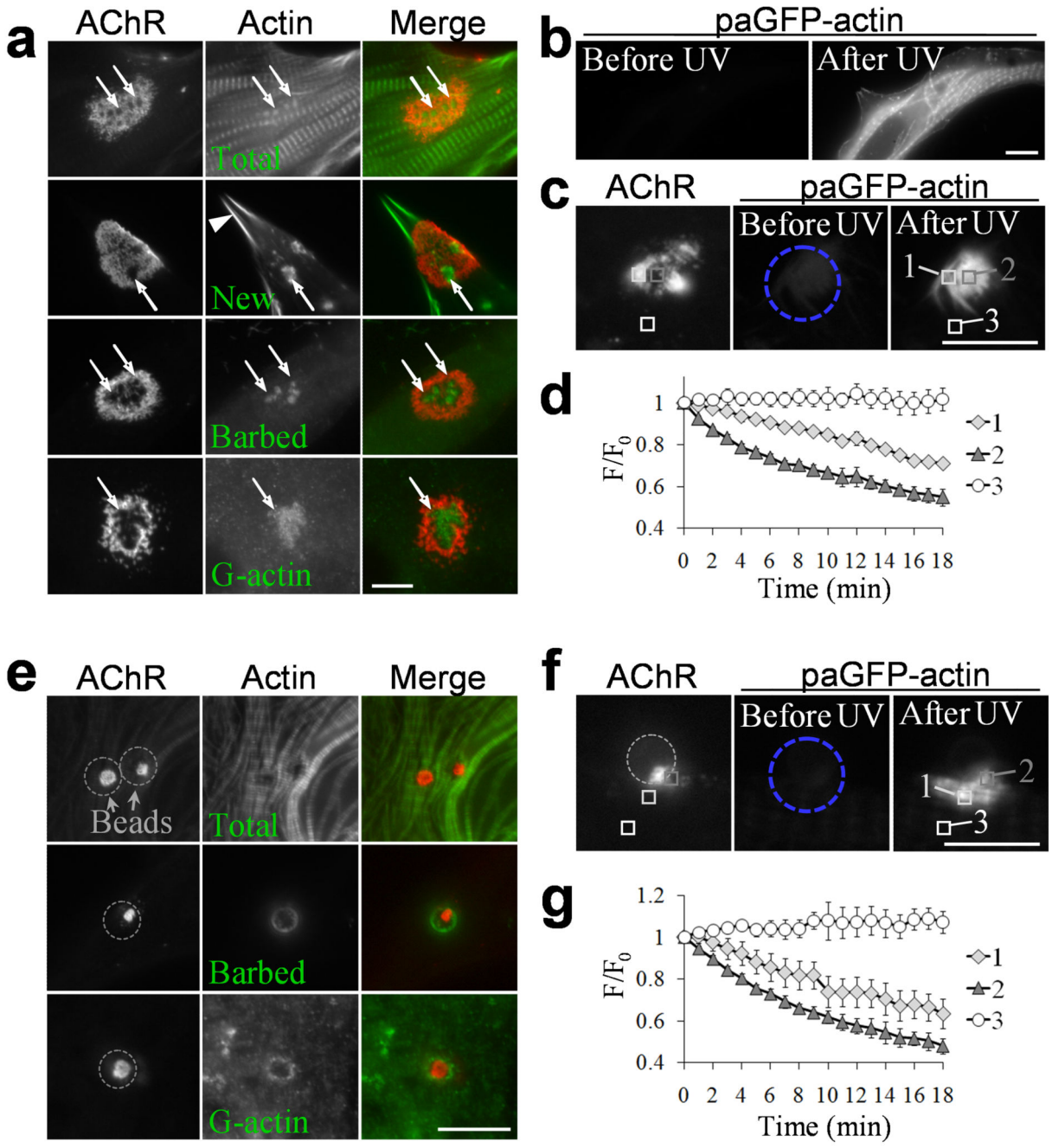

Figure 3. Regulation of actin dynamics by ADF/cofilin in spontaneous and synaptic AChR clusters

(**a**) Actin dynamics in the spontaneous AChR clusters as studied by dissecting different forms of F-actin: total F-actin, newly polymerized F-actin, actin barbed ends, and G-actin (top to bottom rows). Arrows: enrichment of F-actin in the AChR clusters; arrowhead: cell periphery. (**b** – **d**) Actin dynamics as revealed by paGFP-actin photoactivation. A cultured muscle cell expressing paGFP-actin was globally stimulated by UV light, resulting in a dramatic increase in paGFP-actin fluorescence intensity in the whole cell (b). When paGFP-actin was locally activated at a region (blue circle) containing the spontaneous AChR

clusters in a muscle cell (c), fluorescent time-lapse imaging on photoactivated paGFP-actin revealed different rates of changes in fluorescence over time at three different regions as presented in the intensity plot (d; n=4). Analysis boxes: 1, AChR-rich region; 2, AChR-poor perforations; 3, background. (**e**) Spatial distribution of different forms of actin cytoskeleton in cultured muscle cells stimulated with agrin beads for 4 h. (**f**, **g**) Fluorescent images of paGFP-actin photoactivated in a region (blue circle) enclosing the bead-muscle contact (grey circle) in a muscle cell (f). The changes in fluorescence intensity of photoactivated paGFP-actin at three different regions are shown in the intensity plot (g, n=4). paGFP-actin signals in a region adjacent to the bead-induced AChR clusters were found on a different focal plane with that associated with AChR clusters, thus we used paGFP-actin in the striation structure for comparison. Analysis boxes: 1, striation region, 2: region adjacent to the bead-induced AChR clusters; 3: background. Scale bars: 10 μm. Error bars in (d) and (g) represent s.e.m.

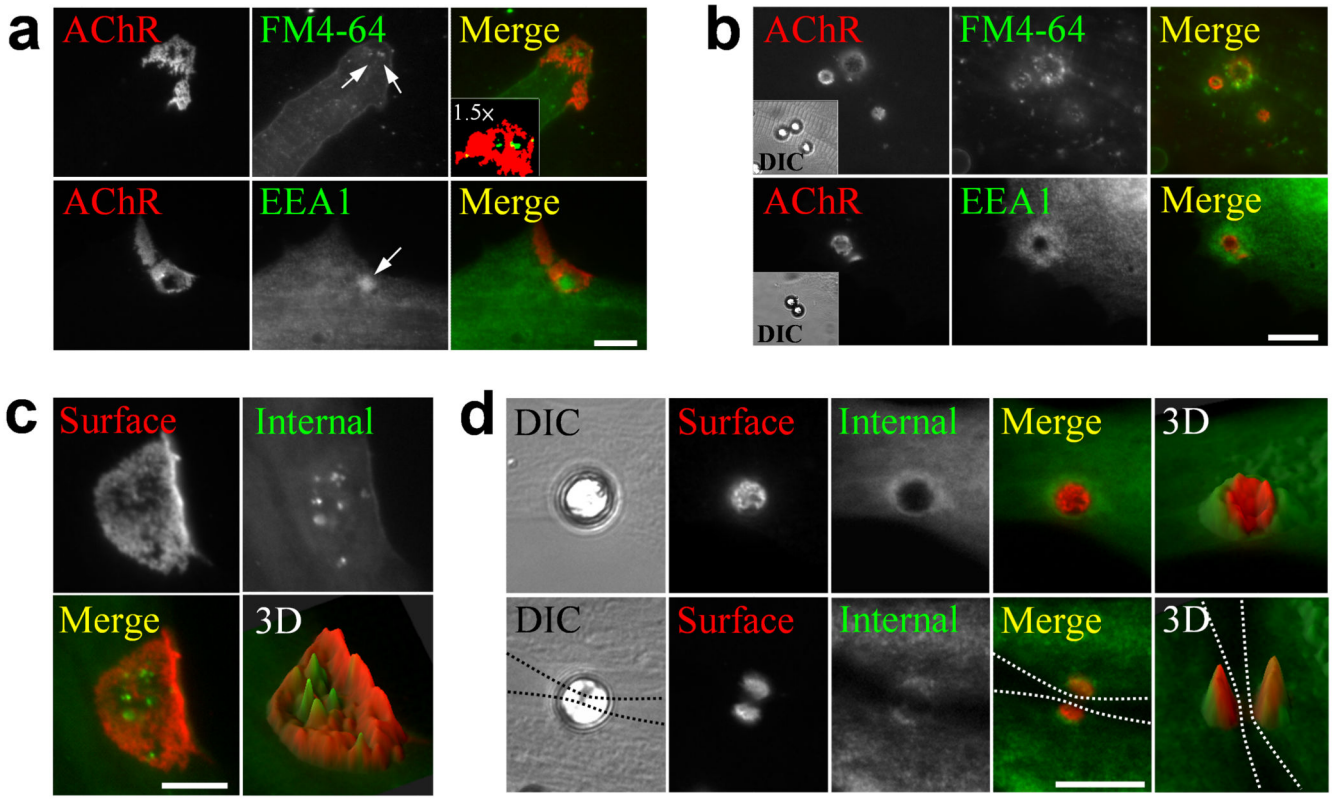

Figure 4. Local enrichment of vesicular trafficking machinery and intracellular AChRs in spontaneous and agrin-induced AChR clusters

(**a**) Vesicular components in spontaneous AChR clusters as labeled with FM4-64 in live cells or EEA1 antibodies in fixed cultures. Pseudo-colored FM4-64 signals were highlighted and magnified in the inset. In the case of double staining with FM4-64, which emits red fluorescence, we used Alexa 488-BTX for AChRs. For the purpose of consistency, we reverted the colors such that FM4-64 is shown as green and AChRs as red. (**b**) Vesicular components surrounding the agrin bead-induced AChR clusters. After 4 h agrin bead stimulation, the muscle cells were stained with either FM4-64 or EEA1 antibodies. Insets: DIC images showing locations of bead-muscle contacts. (**c**, **d**) Surface and internal AChRs as revealed by differential double labeling. Cultured muscle cells were stimulated without (c) or with (d) agrin beads for 4 h. Surface AChRs were labeled with Rh-BTX and then saturated with unlabeled BTX. The cells were fixed, permeabilized and then the intracellular pool of AChRs (internal) was labeled with Alexa 488-BTX. Dotted lines represent the periphery of the cells where an agrin bead landed between two muscle cells. The spatial segregation of surface and internal pools of AChRs was clearly presented in the 3D intensity plots of their fluorescence intensities in the last column of each panel. Scale bars: 20 μm (a); 10 μm (b-d).

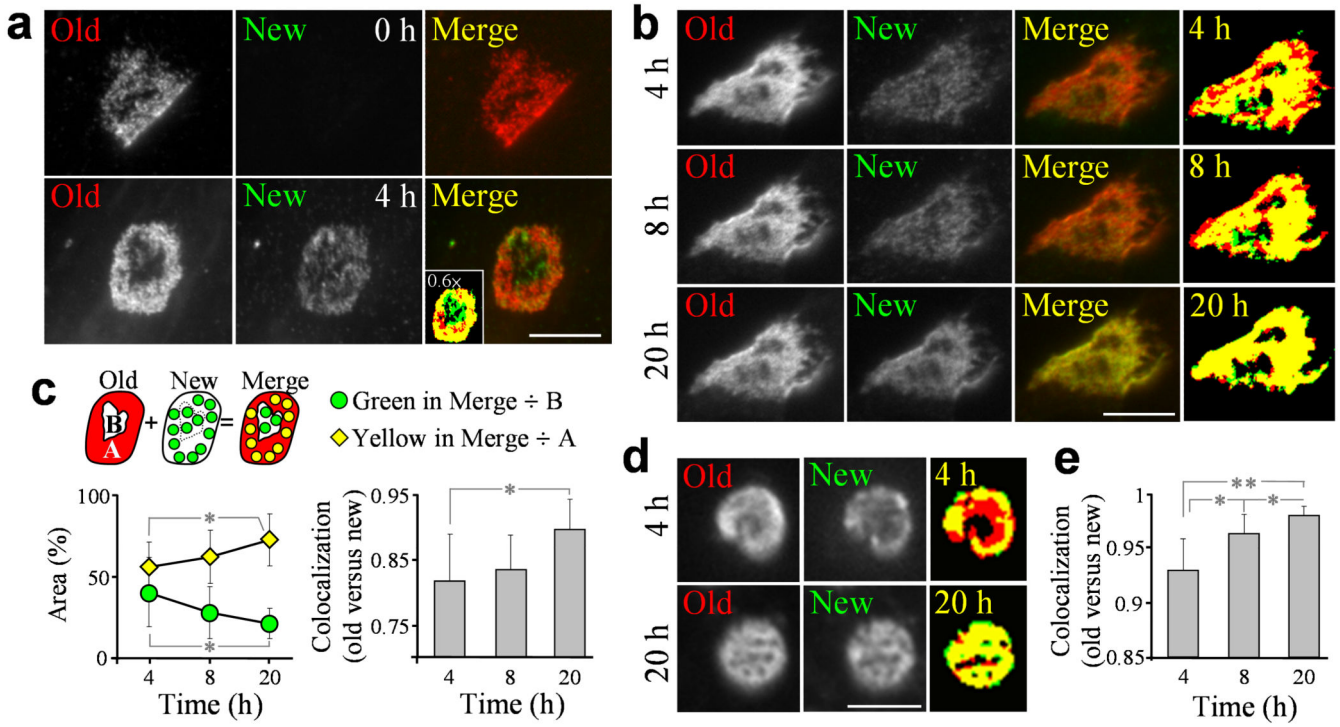

Figure 5. Time-dependent incorporation of newly inserted AChRs into the existing surface AChR clusters

(**a**) Existing and new AChRs as revealed by sequential double labeling. The existing AChRs (Old) were first labeled with Rh-BTX followed by a saturating dose of unlabeled BTX. After 0 or 4 h, newly inserted AChRs (New) were labeled with Alexa 488-BTX. Inset: a merged image of old and new AChRs highlighted by pseudocolors after an intensity threshold. (**b**) Paired images showing old and new AChRs at multiple time points after the sequential double labeling. (**c**) Quantification of the time-dependent incorporation of new AChRs into the old AChR clusters. A: area of the old AChR clusters. B: AChR-poor perforated regions in the clusters. The percentage of area with new AChRs at the perforated region (Green in Merge ÷ B) and the percentage of area with new AChR insertion and/or incorporation into existing AChR region (Yellow in Merge ÷ A) were plotted. Pearson's co-localization coefficients between old and new AChR clusters at different time points were plotted. (**d**) Representative images showing old and new AChR clusters at the agrin bead contact. Paired images of old and new AChR clusters were taken at 4 and 20 h. (**e**) Pearson's co-localization coefficients between old and new AChR clusters at multiple time points were plotted. Asterisks indicate significant differences (*t*test, * $p < 0.005$; ** $p < 0.001$). Scale bars: 20 μm (a, b); 5 μm (d). Error bars in (c) and (e) represent s.e.m.

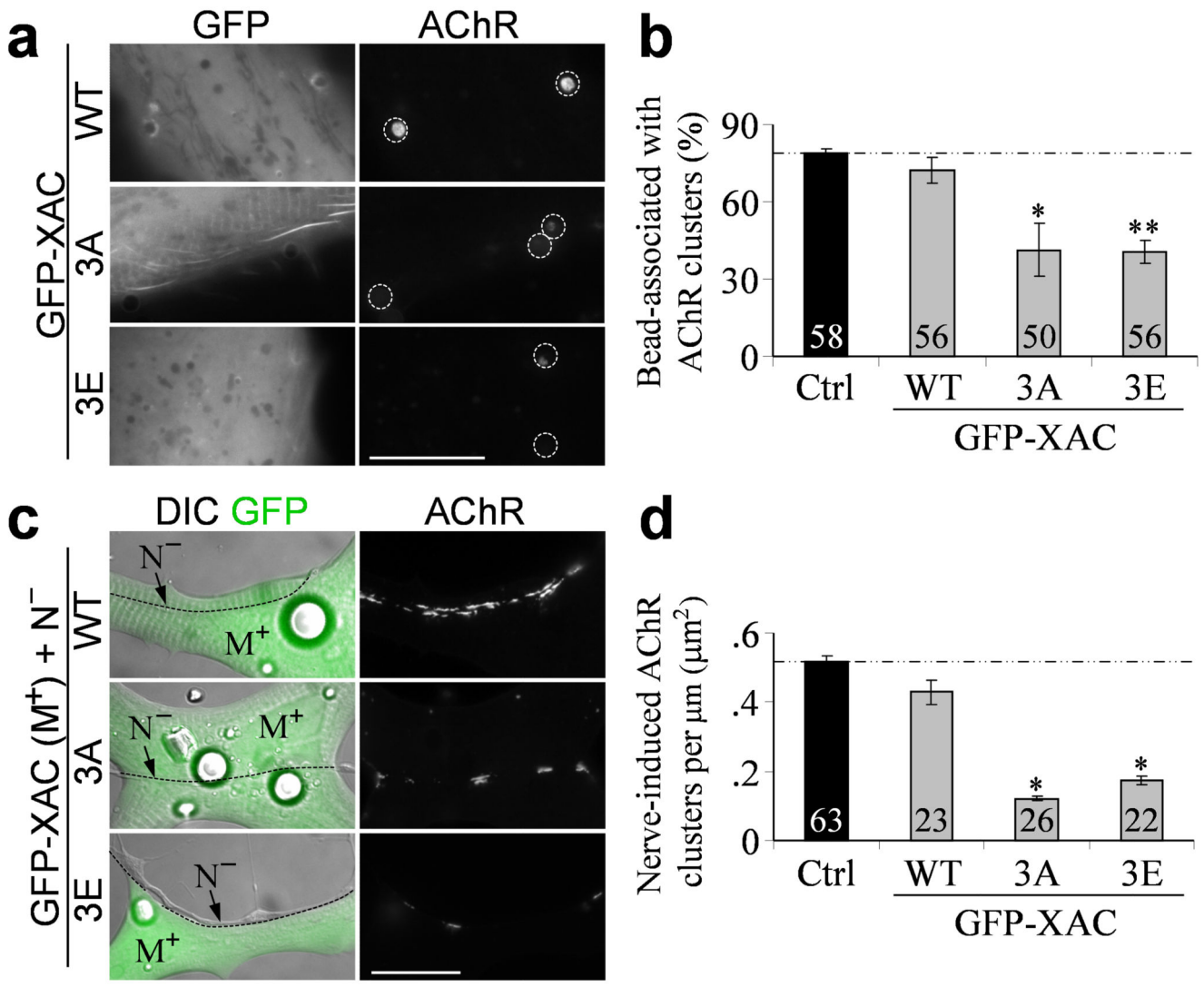

Figure 6. Regulation of agrin- and nerve-induced AChR clustering by ADF/cofilin activity

The cultured muscle cells over-expressed with wild-type or serine-3 phosphorylation mutant forms of GFP-XAC were stimulated with agrin beads (a, b) or spinal neurons (c, d). (**a**) A representative set of images showing AChR clusters induced by 4 h agrin bead stimulation in GFP-expressing muscle cells. Locations of agrin beads were outlined with dotted circles. (**b**) Quantification of the effects of XAC activity on agrin-induced AChR clustering. The percentage of agrin beads in association with those markers were scored if the respective markers were enriched at or around the bead contact sites. (**c**) A representative set of images showing AChR clustering on GFP-XAC-expressed muscles (M^+) induced by co-culturing with wild-type spinal neurons (N^-) for 1 d. The nerve-muscle contacts were outlined with dotted lines for clarity. (**d**) Quantification of the effects of XAC activity on nerve-induced AChR clustering by plotting the area of nerve-induced AChR clusters per a unit length of nerve-muscle contact. Numbers indicate the number of bead-muscle contacts (b) or nerve-muscle contacts (d) counted from at least 3 independent experiments. Asterisks indicate

significant differences (*t*-test, * $p < 0.005$; ** $p < 0.001$). Scale bars: 20 μm. Error bars in (b) and (d) represent s.e.m.

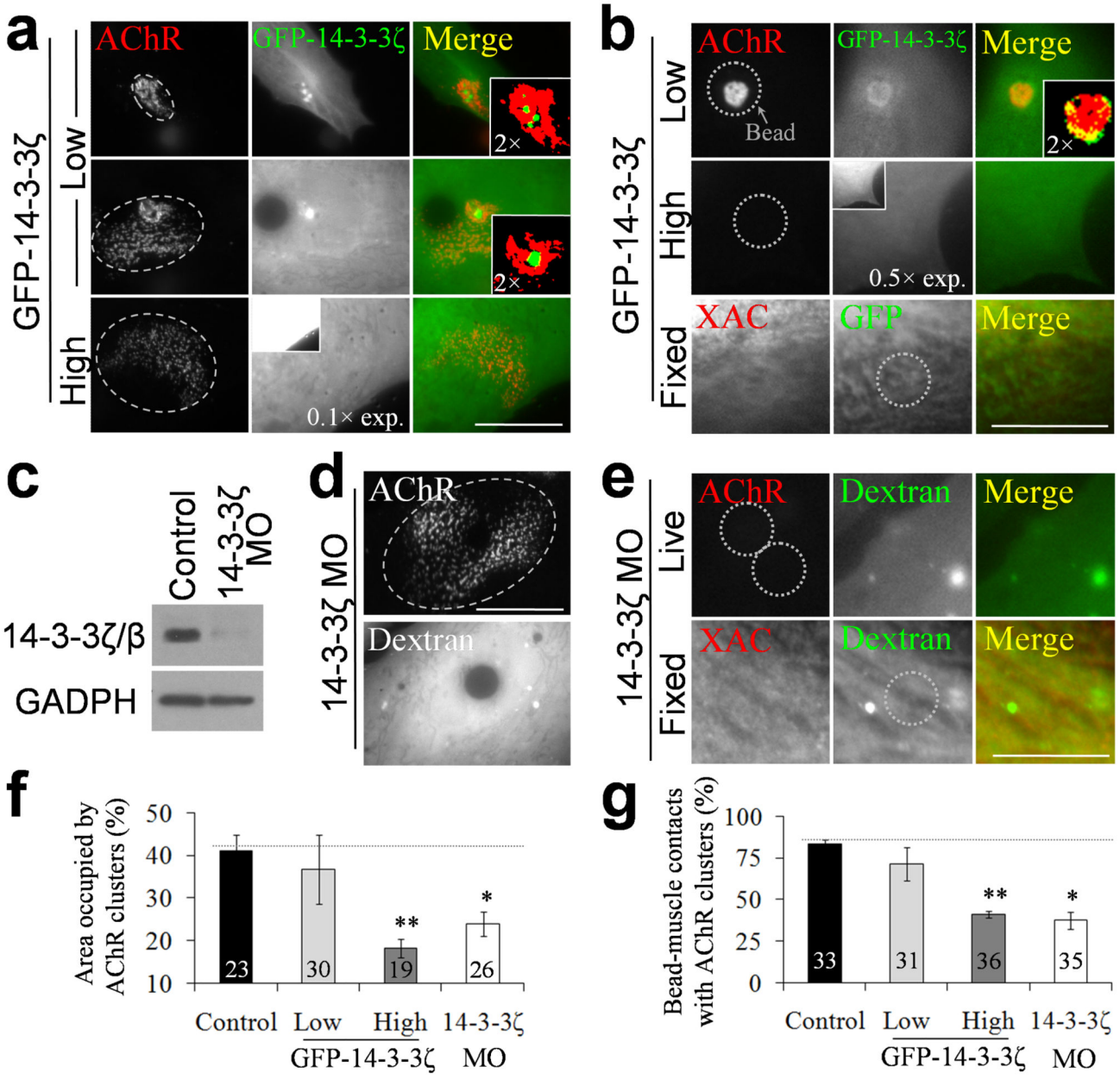

Figure 7. Involvement of 14-3-3ζ in AChR clustering and ADF/cofilin localization. (a, b)

Representative sets of images showing the effects of different over-expression levels of GFP-14-3-3ζ on spontaneous (a) and agrin bead-induced (b) AChR clusters. Please note that the images of high GFP-14-3-3ζ expressing cells were taken using a reduced exposure to allow the examination of subcellular localization. The insets represent the images of the same cells, but acquired using the same exposure as that for cells expressing a low level of GFP-14-3-3ζ. One thus can appreciate the huge difference in the expression level of GFP-14-3-3ζ between these two groups. The magnified regions were pseudo-colored after an intensity threshold to show the differential localization of GFP-14-3-3ζ and AChRs (color insets). XAC immunostaining was performed in GFP-14-3-3ζ-expressed muscle cells

stimulated with agrin beads. (**c**) Western blotting analysis on the 14-3-3ζ/β protein levels in the 14-3-3ζ morpholino (MO) knockdown experiment with GADPH as a loading control. Full-length blots are presented in Supplementary Fig. 12. (**d**) A similar disorganization of the spontaneous AChR clusters cultured from 14-3-3ζ morpholino embryos, as identified by fluorescent dextran signals. Ellipses (a, d) were drawn to outline the periphery of AChR clusters for the quantitative analysis in panel f. (**e**) A representative set of images showing the effects of 14-3-3ζ morpholino on AChR clustering and XAC localization induced by agrin beads. (**f**, **g**) Quantifications of spontaneous (f) and agrin bead-induced (g) AChR clusters in response to 14-3-3ζ over-expression or morpholino knockdown. Numbers indicate the number of samples counted from 2 independent experiments. Asterisks indicate significant differences (*t*-test, * $p < 0.005$; ** $p < 0.001$). Scale bars: 20 μm (a, d); 10 μm (b, e). Error bars in (f) and (g) represent s.e.m.

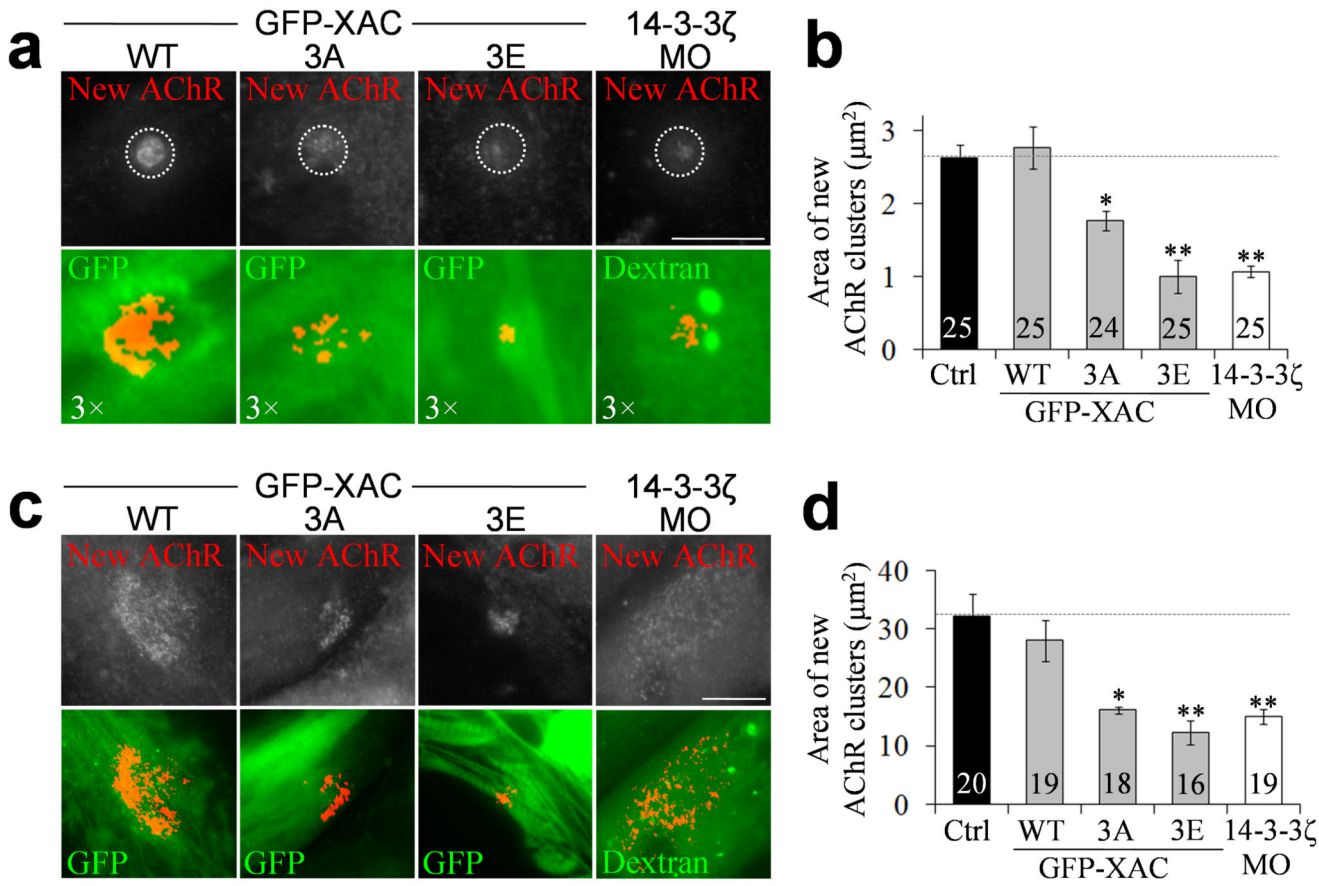

Figure 8. Regulation of surface targeting of new AChRs by ADF/cofilin activity and 14-3-3ζ

(**a**, **c**) Representative images showing newly inserted AChRs in agrin bead-induced (a) or spontaneous (c) AChR clusters in muscle cells expressing different XAC or 14-3-3ζ morpholino knockdown. The pre-existing surface AChRs were first masked with a saturating dose of unlabeled BTX. After 4 h, the cells were labeled with Rh-BTX and fixed to allow precise and reliable quantification of the newly inserted AChRs (New AChR) in a large number of cells at this particular time point. The muscle cells over-expressing wild-type or mutants of GFP-XAC were identified by GFP expression, whereas 14-3-3ζ morpholino knockdown was identified by fluorescent dextran signals. It should be noted that the exact subcellular localization of GFP-tagged proteins may be altered after fixation. The area of new AChRs was highlighted with red pseudocolors through the application of an intensity threshold in merge images (bottom rows). Locations of agrin beads were outlined with dotted circles in top panels. (**b**, **d**) Quantifications of XAC activity and 14-3-3ζ manipulations on surface targeting of new AChRs in agrin-induced (b) or spontaneous clusters (d). Areas of new AChR clusters at the bead-muscle contacts and at the spontaneous clusters were measured in the threshold images. Numbers indicate the number of bead-muscle contacts (b) or spontaneous clusters (d) measured from 2 independent experiments. Asterisks indicate significant differences (*t*-test, * $p < 0.005$; ** $p < 0.001$). Error bars in (b) and (d) represent s.e.m.